

Table of contents:

Supplementary Figures:

- Figure S1. Energy diagrams of fluorescence-encoded IR (FEIR) and stimulated Raman excited fluorescence (SREF).
- Figure S2. Simulation of BonFIRE process with a three-level system.
- Figure S3. Dependence of the BonFIRE background and signal-to-background ratios (S/B) on the probe wavelength for ATTO680.
- Figure S4. Raw data and fittings in **Fig. 3e**.
- Figure S5. UV-vis spectra of four BF1 isotopologues.
- Figure S6. The single-molecule behaviour and bulk BonFIRE spectra of ATTO680 and Rh800.
- Figure S7. Representative fluorescence images and photobleaching curves of single-molecule samples.
- Figure S8. Photo-stability of biological BonFIRE microscopy.
- Figure S9. Comparison between BonFIRE and photothermal (PT) spectra.
- Figure S10. Sample movement during live-cell imaging.
- Figure S11. Characterization for the temporal buildup of the photothermal background.
- Figure S12. Modulation scheme of background-free BonFIRE microscopy.
- Figure S13. BonFIRE lifetime imaging microscopy (BLIM).
- Figure S14. Linewidth, peak position, and lifetime measurements of the 1300 cm^{-1} peak for Rh800 in different solvents.
- Figure S15. Widefield BonFIRE microscopy.

Supplementary Tables:

- Table S1. Measured vibrational peaks of dyes.
- Table S2. BonFIRE signal comparison of dyes with C=C modes.
- Table S3. Molecular structures of dyes used in BonFIRE.
- Table S4. BonFIRE signal comparison of dyes with C≡C and C≡N modes conjugated to the dye systems.
- Table S5. Comparisons of key parameters of bioimaging between BonFIRE, SREF, and FEIR.

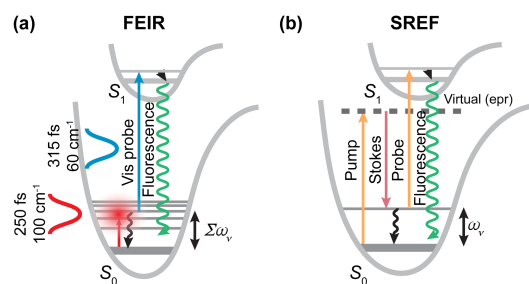


Figure S1. Energy diagrams of fluorescence-encoded IR (FEIR, a) and stimulated Raman excited fluorescence (SREF, b). Adapted from refs.^{1,2}, respectively.

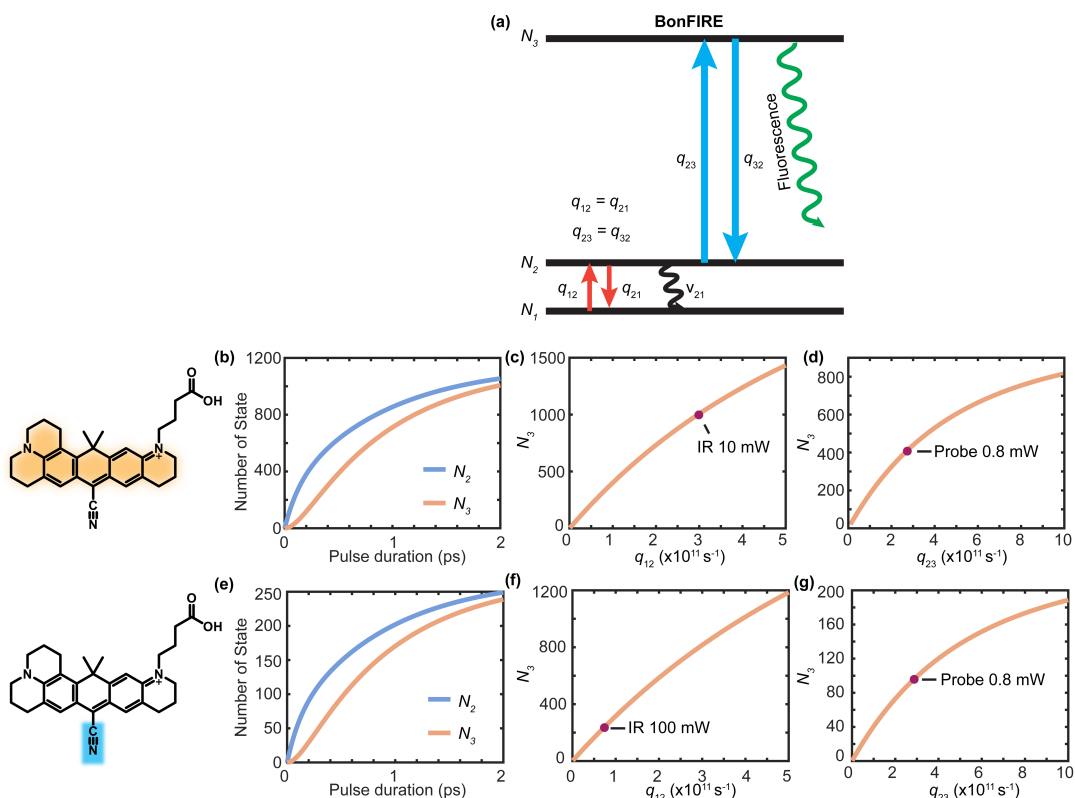


Figure S2. Simulation of BonFIRE process with a three-level system. (a) The energy diagram for the three-level system simulation. Two scenarios – one with C=C excitation (orange-shade highlighted in the second row, b-d) and the other with C≡N excitation (blue-shade highlighted in the third row, e-g) in BF1 dye molecule – were numerically simulated. In the simulation, the initial ground-state population (N_1) is set to 10000, and the number of steps of the population evolution is set to 50000, corresponding to 4×10^{-5} ps per step. (b)&(e) Population changes in N_2 and N_3 during 2-ps pulse duration. (c-d)&(f-g) Electronic excited-state population (N_3) as functions of IR transition rate of q_{12} and probe transition rate of q_{23} . Fixing all other parameters (pulse duration, wavelength, Franck-Condon constant, etc.), q_{12} and q_{23} are pure functions of IR and probe powers. IR powers used for simulation in (b)&(e) and probe powers reaching the saturation level are indicated by red dots. For the formulae of the simulation, please see the “Modeling of the double-resonance in BonFIRE” in **Methods**.

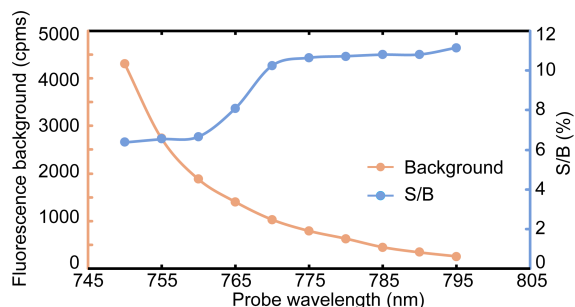


Figure S3. Dependence of the BonFIRE background and signal-to-background ratios (S/B) on the probe wavelength for ATTO680. The BonFIRE background increases as the combined excitation frequency of the probe and the IR (at 1598 cm^{-1}) gets closer to the absorption peak (681 nm), leading to a drop in S/B at the probe wavelength lower than 775 nm. To strike a balance between the signal intensity, signal-to-noise ratio (S/N), and S/B, we choose 765 nm for BonFIRE spectroscopy. The sample here is $1\text{ }\mu\text{M}$ ATTO680 in DMSO. The on-sample powers are $350\text{ }\mu\text{W}$ of the probe and 40 mW of the IR (1598 cm^{-1}). SPCM readings (cpms: photon counts per ms) were corrected based on the calibration curve provided by the manufacturer (Excelitas).

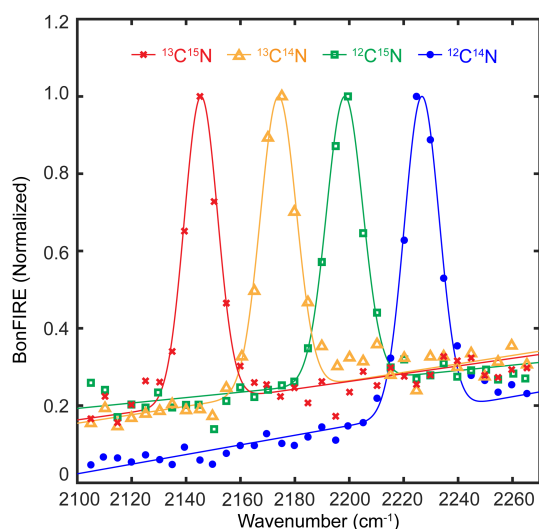


Figure S4. Raw data and fittings in Fig. 3e. The fittings were performed with a Gaussian function and a linear background for each colour-coded spectrum.

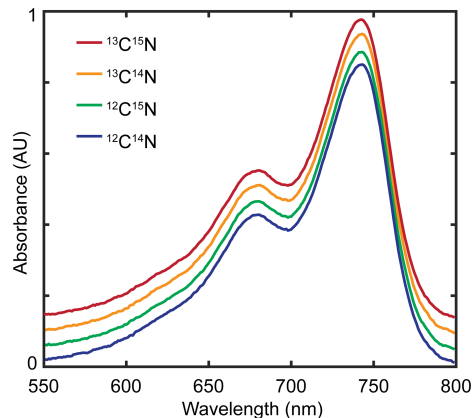


Figure S5. UV-vis spectra of four BF1 isotopologues. Four absorption spectra and peaks (758 nm) of BF1 dyes with $^{13}\text{C}\equiv^{15}\text{N}$, $^{13}\text{C}\equiv^{14}\text{N}$, $^{12}\text{C}\equiv^{15}\text{N}$, and $^{12}\text{C}\equiv^{14}\text{N}$ are almost identical in 10 μM DMSO solutions. Absorption profiles are vertically shifted for better comparison.

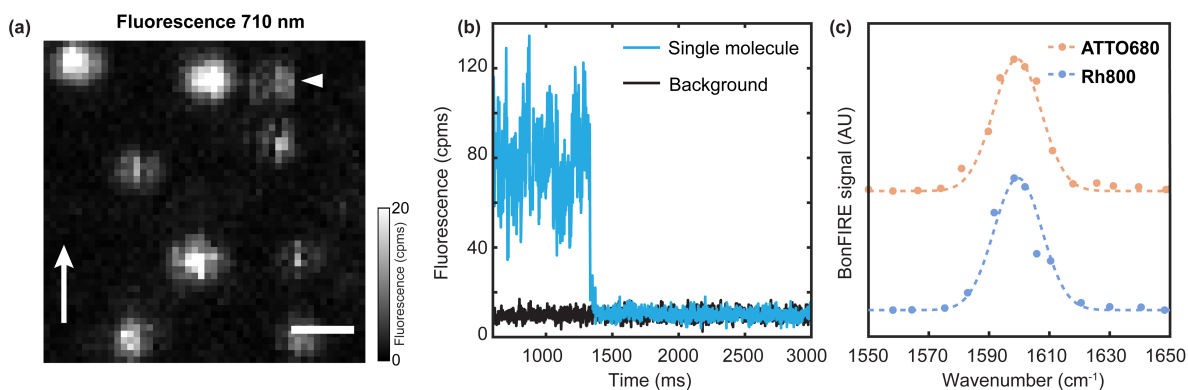


Figure S6. The single-molecule behaviour and bulk BonFIRE spectra of ATTO680 and Rh800. (a-b) Representative fluorescence image (a) and single-step photobleaching curve (b) for confirming the single-molecule sample preparation. In (a), the white arrow on the left shows the scan direction, and the white arrowhead indicates the “half-moon” bleach of a single molecule. cpms: counts per millisecond. Cpms: counts per millisecond. Scale bar: 1 μm . (c) BonFIRE spectra of C=C modes in ATTO680 and Rh800 from dried dye/PVA aggregates. Spectra are vertically shifted for better comparison.

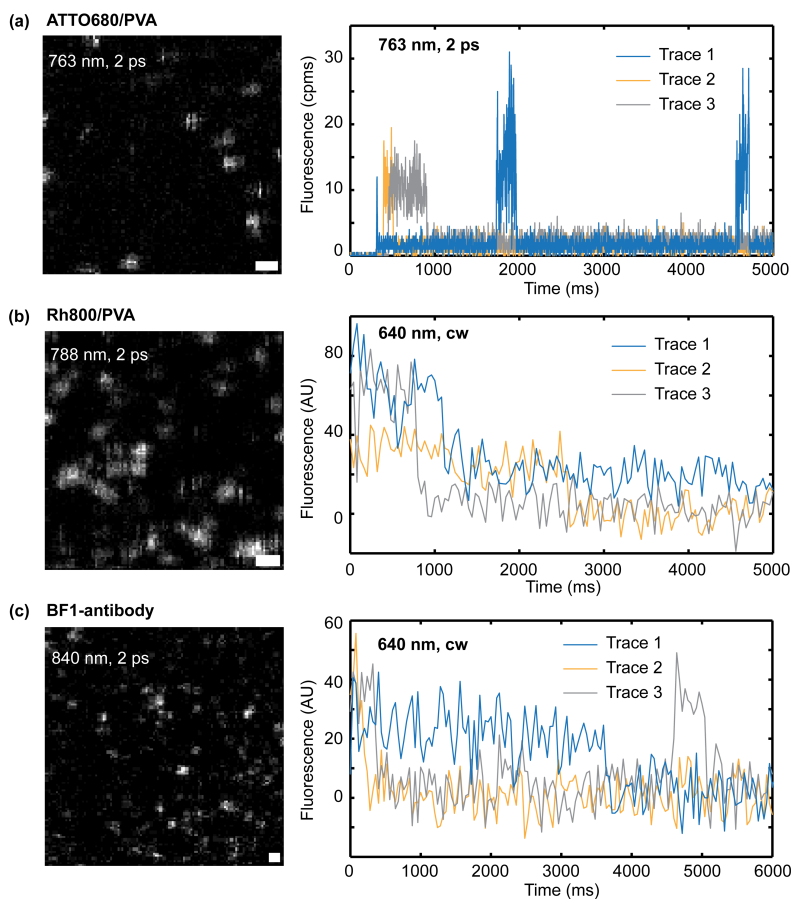


Figure S7. Representative fluorescence images and photobleaching curves of single-molecule samples. Representative fluorescence images and photobleaching curves (three representative curves for each sample) are obtained for ATTO680 (a), Rh800 (b), and BF1-antibody conjugates (c). Single-step bleach and blinking could be observed in photobleaching curves, indicating the presence of single molecules. For (a) and (b), single-molecule samples were prepared by spin casting 20 pM ATTO680 or 10 pM Rh800 in 0.2% PVA solution onto a new CaF₂ window using 5000 rpm for 30 s. For (c), the single-molecule sample was prepared by incubating dye-antibody conjugates solution (diluted 625000 times in PBS from a 0.5 mg/mL stock solution, the dye:protein ratio is 1.7:1) onto a poly-L-lysine coated CaF₂ window for 30 min, and then dried in air before imaging. For ATTO680 with a high quantum yield (30%), the probe wavelength (763 nm, 2 ps) used for BonFIRE can be directly applied to performing *in-situ* photobleaching, while the fluorescence photon counts were recorded over time through the SPCM with a binning width (temporal step) of 2 ms. For Rh800 and BF1, however, the quantum yield is low (16% and 10%), and the wavelength of BonFIRE probe (788 nm and 840 nm) is too red to obtain reproducible bleach curves. We instead obtained bleach curves of the same samples using a commercial confocal microscope (Olympus FV3000) with a 640-nm cw excitation and detected the fluorescence change over time using PMT. Each step is 40 ms in (b) and (c). The PMT offset is corrected so that the fluorescence baseline is zero. 0.2 mW at 763 nm for ATTO680 and 5 mW at 640 nm for Rh800 and BF1 were used for obtaining photobleaching curves. Cpms: counts per millisecond. Scale bars: 1 μ m.

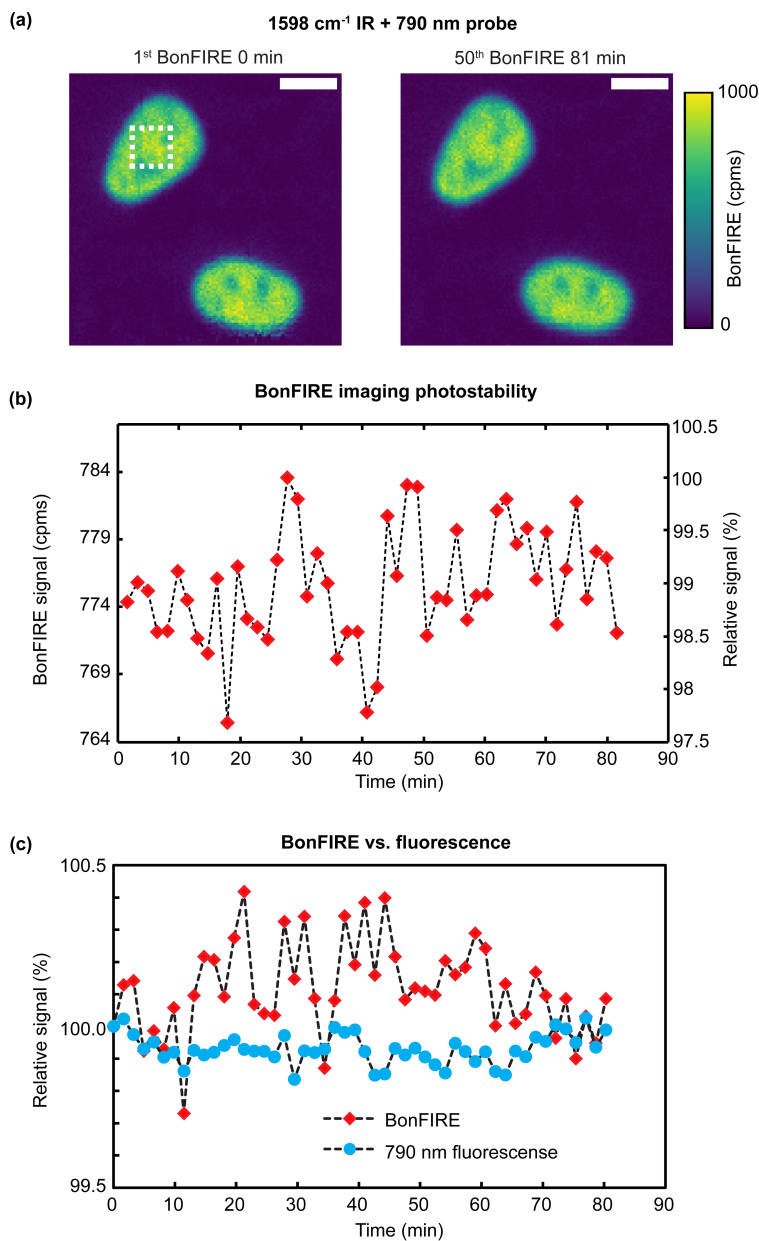


Figure S8. Photo-stability of biological BonFIRE microscopy. ATTO680-click-labelled-EdU cells on CaF₂ were imaged with on-sample IR power of 21 mW and probe power of 2 mW over 100-frame consecutive image scans. BonFIRE images were obtained by subtracting two adjacent frames captured at 0-ps and 20-ps probe-IR delays. (a) The first and the last (50th) BonFIRE images of ATTO680 C=C showing two cell nuclei. The average signal from a cropped area (indicated by a white dashed box in the first image) is plotted against time in (b), where the BonFIRE signal oscillates between 97.5% and 100%. (c) Comparison of photobleaching between probe-only fluorescence and BonFIRE under the same power and imaging condition, confirming that introducing an additional IR beam does not increase the photobleaching rate in BonFIRE as compared to that of the probe-only fluorescence. Cpms: counts per millisecond. Scale bars: 10 μ m.

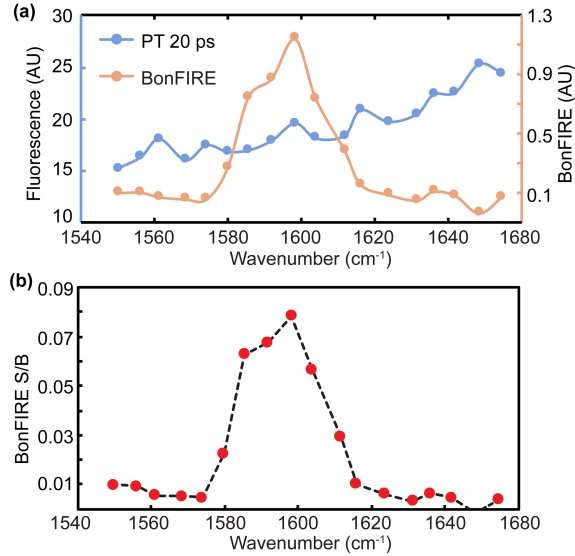


Figure S9. Comparison between BonFIRE and photothermal (PT) spectra from a 100 μM ATTO680 DMSO solution. While the BonFIRE spectrum shows the 1598 cm^{-1} peak of ATTO680 explicitly, the photothermal spectrum at $t_D=20$ ps is featureless. The S/Bs across frequencies are plotted in (b).

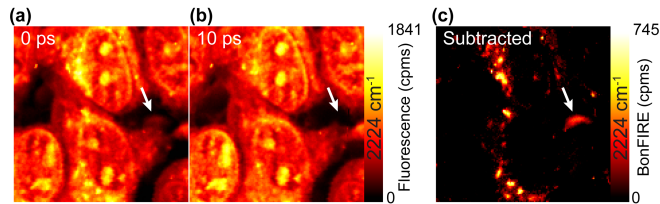


Figure S10. Sample movement during live-cell imaging. C \equiv N BonFIRE imaging of Rh800-stained live HeLa cells at IR-probe delays (t_D) of 0 ps (a), 10 ps (b), and after subtraction (c). The time for capturing each frame was ~ 40 s. The first two images were acquired consecutively using SPCM. The arrow indicates the subtraction artefact in (c) caused by cell movement. Cpms: counts per millisecond.

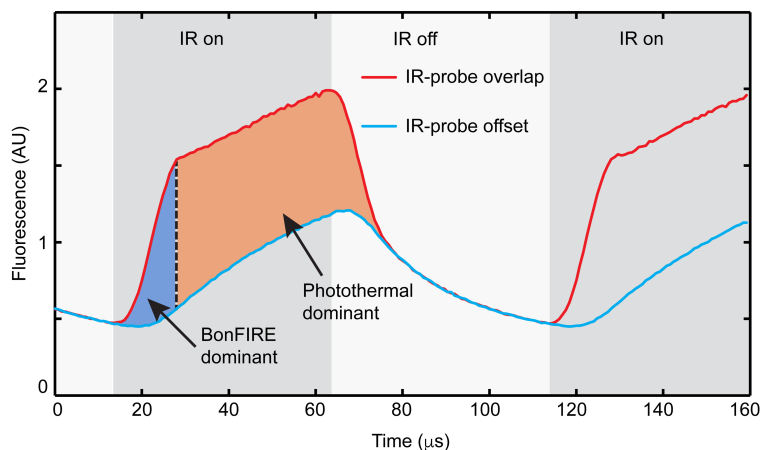


Figure S11. Characterization for the temporal buildup of the photothermal background.

BonFIRE intensity measured by PMT is plotted against time, as the IR beam is chopped at 10 kHz. When the IR and probe are temporally overlapped (red curve), a fast-increasing component in the BonFIRE signal (the blue-shaded area) could be observed, followed by a slow-increasing component due to the temperature rise caused by the IR-photothermal effect. When the IR and probe are temporally separated (blue curve), only the slow-increasing component is seen, resulting from the pure photothermal effect. The orange-shaded area indicates the photothermal-induced BonFIRE background rises at the time scale of tens of μs , while the initial BonFIRE signal burst stops within several μs (blue-shaded area). Note that the slow increase of BonFIRE-dominant fluorescence signal around 20 μs is mostly caused by the slow chopper movement and data acquisition and does not accurately indicate the temporal generation of BonFIRE signals.

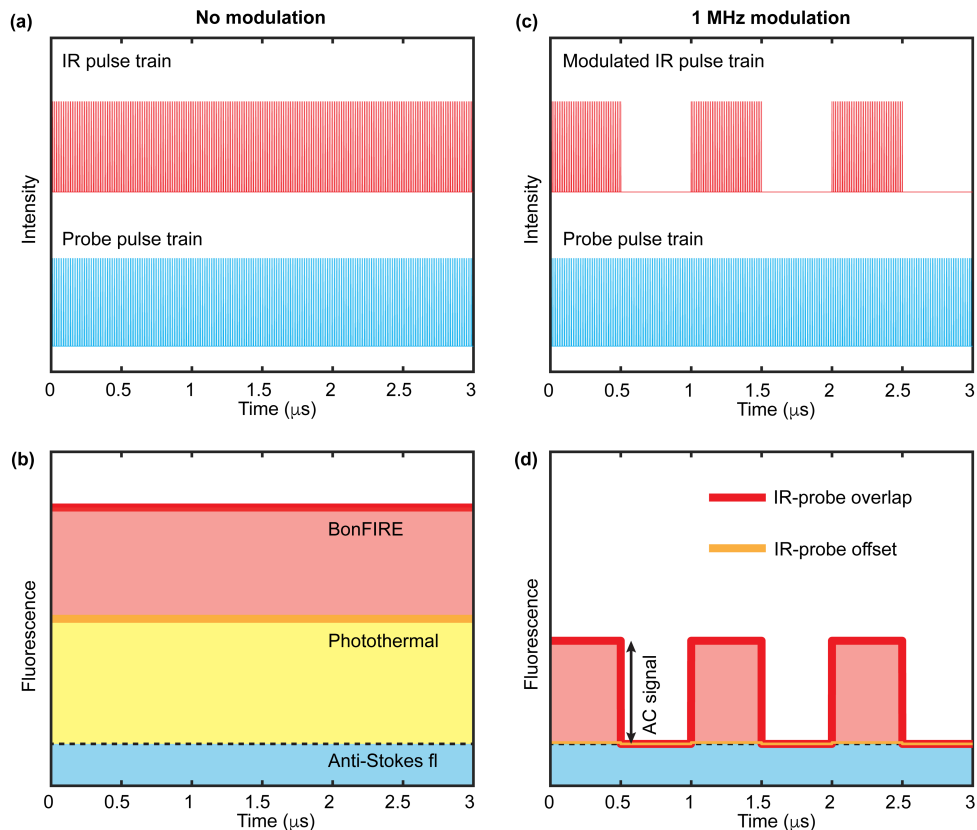


Figure S12. Modulation scheme of background-free BonFIRE microscopy. (a-b) Simulated pulse trains (a) and the expected total signal (b) when IR pulses are not modulated. The total signal is composed of anti-Stokes fluorescence (blue shaded) detected with probe laser alone, IR-induced photothermal fluorescence (yellow shaded) detected when IR and probe are temporally offset, and BonFIRE signal (red shaded) detected when IR and probe are temporally overlapped. (c-d) Simulated pulse trains (c) and the expected signal (d) when 80 MHz IR pulse trains are intensity-modulated by AOM at 1 MHz. The first-order diffraction from AOM completely turns off the IR throughput and achieves maximal on/off ratios. Due to the high-frequency modulation, the photothermal background has no time to build up (**Fig. S11**) and is almost completely suppressed, and the anti-Stokes fluorescence is removed through the lock-in demodulation (d).

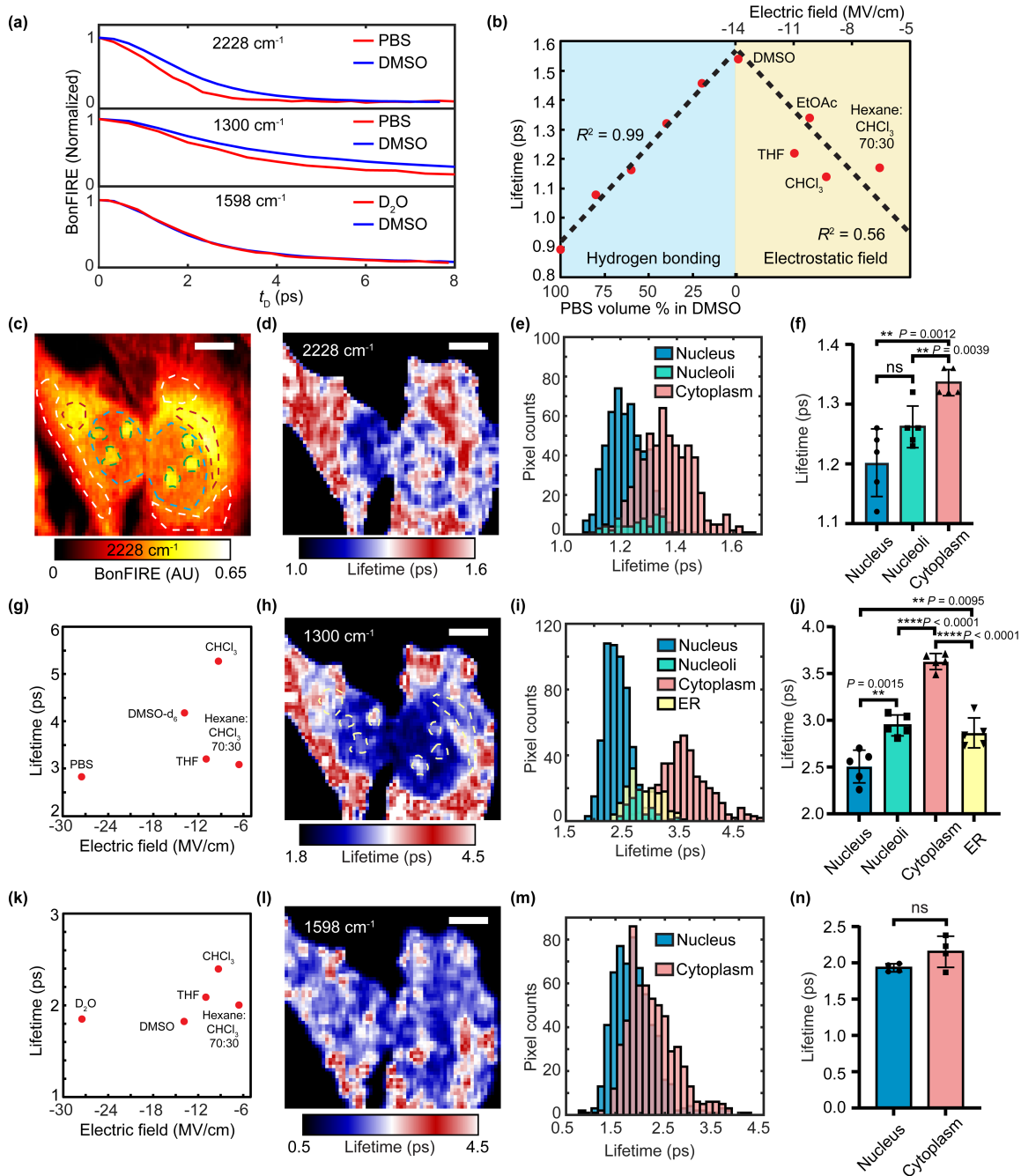


Figure S13. BonFIRE lifetime imaging microscopy (BLIM). (a) BonFIRE signal dependence on IR-probe temporal delay measured for $\text{C}\equiv\text{N}$ (2228 cm^{-1}), aromatic C-N (1300 cm^{-1}), and C=C (1598 cm^{-1}) of Rh800 in water and DMSO environments. While both $\text{C}\equiv\text{N}$ and C-N show different lifetimes in water and DMSO, the lifetime of C=C is constant between the two environments. (b) Solvatochromism of $\text{C}\equiv\text{N}$ of Rh800 in PBS:DMSO mixture (left, blue-shaded) and different aprotic solvents with varying electrostatic fields (right, yellow-shaded) calculated from Onsager reaction field theory³ (field of PBS was adopted from literature⁴). An inverted “V-shape” is observed in (b), showing the lifetime of $\text{C}\equiv\text{N}$ is an indicator of the Stark effect (right part) and hydrogen-bonding environment (left part). This finding is consistent with the vibrational Stark

effect (VSE) benchmarked with nitrile peak shift,⁵ and the opposite trend in PBS:DMSO mixture due to hydrogen-bonding effects.^{3,4} (c) BonFIRE image of Rh800-stained HeLa cells immersed in PBS obtained at 2228 cm⁻¹. Subcellular regions are indicated by dashed green (nucleus and nucleoli), red (endoplasmic reticulum, ER), and white (cytoplasm, excluding ER) enclosures. (d) BLIM image at 2228 cm⁻¹ for C≡N of the same field of view (FOV). Nucleus and cytoplasm (including ER) regions are clearly differentiated. (e) Histogram of lifetime values in different subcellular regions. (f) Statistics of lifetime measurements. While the C≡N lifetime can differentiate between the nucleus and cytoplasm (**p = 0.0012 unpaired Student's t-test, two-tailed, n = 5), it cannot distinguish the nucleus from nucleoli. Data are presented as mean values +/- SD. (g) Solvatochromism of aromatic C-N (1300 cm⁻¹) lifetime in different solvents. Although a large difference could be found between different solvents (e.g., ~80% increase from PBS to CHCl₃), no linear dependence on the electric field could be established, indicating a different sensing mechanism from C≡N. (h) BLIM image at 1300 cm⁻¹. In addition to the nucleus and cytoplasm, nucleoli and ER (highlighted by white dashed enclosures) could be further distinguished from the nucleus and cytoplasm. (i) Histogram of lifetime values obtained in different subcellular regions. (j) Statistics of lifetime measurements. Clear differences could be found between the nucleus and nucleoli (**p = 0.0015 unpaired Student's t-test, two-tailed, n = 5) and between ER and cytoplasm (****p < 0.0001 unpaired Student's t-test, two-tailed, n = 5). Compared to C≡N, C-N is more sensitive to differentiating nucleoli from nuclei. Moreover, with a positive charge in the resonant structure, aromatic C-N is likely more sensitive to varied charged membrane environments so that the ER could be distinguished by BLIM. Data are presented as mean values +/- SD. (k) Solvatochromism of conjugated C=C (1598 cm⁻¹). The lifetimes are highly close in different solvents, indicating that C=C is less sensitive in sensing. (l) BLIM image at 1598 cm⁻¹, no clear contrast could be extracted between different subcellular regions. (m) Histogram of lifetime values obtained in nucleus and cytoplasm, showing a small difference. (n) Statistics of lifetime measurements. No difference (ns = not significant, unpaired Student's t-test, two-tailed, n = 5) could be found between the nucleus and cytoplasm, indicating the C=C is the least sensitive mode among the three modes. Data are presented as mean values +/- SD. Scale bars: 10 μm.

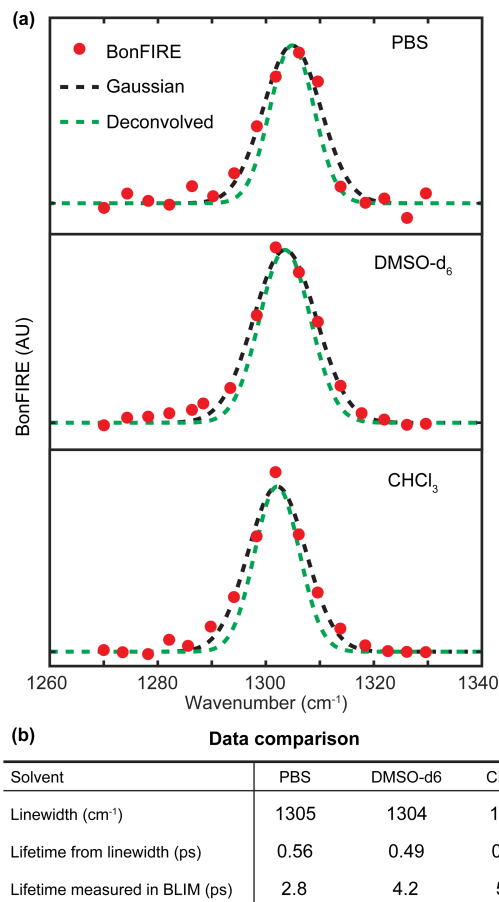


Figure S14. Linewidth, peak position, and lifetime measurements of the 1300 cm⁻¹ peak for Rh800 in different solvents. (a) To fit and extract the linewidth, we oversampled the BonFIRE spectra with a 4 cm⁻¹ step size, which is half of the IR laser bandwidth (8 cm⁻¹). BonFIRE data were obtained from 100 μM Rh800 in each solvent with probe wavelength fixed at 780 nm. The fitted Gaussian peak (black dashed curve) is deconvolved with the laser bandwidth with 8 cm⁻¹ full width at the half maximum (FWHM), and the result is shown as the green dashed curve. The peak position, FWHM, lifetime calculated from the FWHM assuming the lifetime-broadening, and lifetime measured directly by BLIM are summarized in (b). The lifetime measured by BLIM is significantly longer than that calculated from linewidth, indicating the 1300 cm⁻¹ peak of Rh800 is not lifetime-broadened.

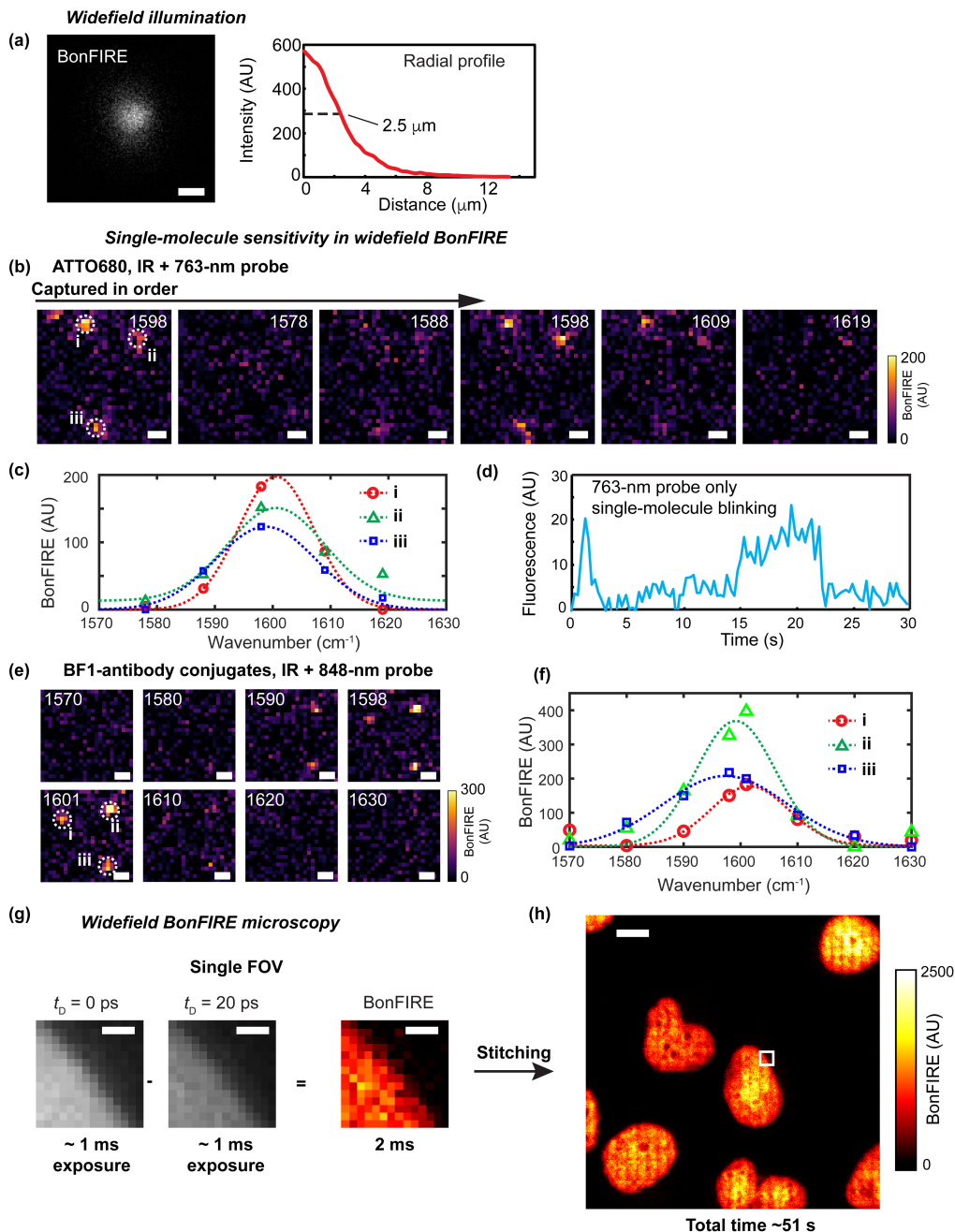


Figure S15. Widefield BonFIRE microscopy. (a) Characterization of illumination area of the widefield BonFIRE microscopy with single-molecule sensitivity. The measured radial profile of BonFIRE indicates a 5 μm BonFIRE spot size. More experimental details in **Methods**. Scale bar: 5 μm . (b) Widefield BonFIRE images of single ATTO680 molecules embedded in PVA matrix. Each BonFIRE frame is a single field of view (FOV) obtained using widefield illumination and 5 s camera exposure time. The clear contrast between on (1598 cm^{-1}) and off (others) frames indicates the single-molecule sensitivity. Three single molecules (i, ii, and iii) are highlighted with dashed circles in the first on-resonance frame. (c) *In-situ* BonFIRE spectra and Gaussian fittings obtained from molecules i, ii, and iii. After the BonFIRE imaging, the same FOV was illuminated with a probe beam with increased power (2 mW on sample) to obtain single-molecule

photobleaching curves. (d) A representative single-molecule blinking time trace obtained from the single molecule i, proving the sample quality. The fluorescence readings were corrected by subtracting the baseline due to the system offset of the sCMOS detector. (e-f) Widefield BonFIRE images of single BF1-conjugated antibodies (e) and representative *in-situ* spectra from three single molecules (labelled as i, ii, and iii in the 1601 cm^{-1} frame, f). Scale bars in (b) & (e): 1 μm . (g-h) Widefield BonFIRE image of ATTO680-EdU-labelled HeLa nucleus at 1598 cm^{-1} . Using an evenly illuminated $3 \times 3 \mu\text{m}^2$ BonFIRE FOV, each FOV can be acquired at the video rate (e.g., 2 ms per frame, g) and stitched together to form a large-area BonFIRE image (h). The stitched large-area ($87 \times 87 \mu\text{m}^2$) image with 406×406 pixels was captured within 51 s, about 30 times faster than using the point-scan scheme with same parameters (i.e., pixel size and dwell time). We note here the imaging speed for the stitching is limited by the movement speed of the piezostage and the time needed for the synchronization between the camera and PC using a customized LabVIEW code (~ 60 ms per step), not by the imaging acquisition speed (2 ms per frame). The scanning and stitching speed could be further improved by enlarging the FOV. Scale bars are 1 μm in (g) and 10 μm in (h).

Table S1. Vibrational peaks of dyes.

Dye	Absorption peak (nm)	Vibrational peaks (cm ⁻¹)
Coumarin-6	444	817, 941, 1014, 1078, 1134, 1190, 1261, 1350, 1413, 1512, 1589, 1614, 1714
Nile Blue A	635	858, 947, 1008, 1074, 1106, 1171, 1257, 1275, 1332, 1375, 1438, 1549, 1584
Cy5	646	961, 1007, 1106, 1155, 1220, 1298, 1316, 1373, 1407, 1439, 1469, 1496
ATTO647N	646	1003, 1134, 1206, 1274, 1317, 1406, 1439, 1483, 1598, 1693
Alexa Fluor 647	647	1006, 1110, 1145, 1215, 1385, 1470, 1500
ATTO665	662	984, 1004, 1203, 1313, 1429, 1472, 1598
BF2	680	997, 1071, 1160, 1184, 1198, 1258, 1285, 1325, 1340, 1407, 1440, 1515, 1603, 1663, 1695, 2228 (¹² C≡ ¹⁴ N)
Alexa Fluor 680	681	991, 1091, 1122, 1205, 1307, 1374, 1465, 1508, 1576
ATTO680	681	982, 1024, 1038, 1074, 1142, 1168, 1286, 1334, 1402, 1477, 1521, 1598, 1650, 1722
Cy5.5	684	1124, 1157, 1361, 1463, 1489
Rh800	695	1102, 1184, 1208, 1301, 1361, 1379, 1461, 1508, 1544, 1598, 2142 (¹³ C≡ ¹⁵ N), 2174 (¹³ C≡ ¹⁴ N), 2198 (¹² C≡ ¹⁵ N), 2222 (¹² C≡ ¹⁴ N)
BF3	696	1000, 1079, 1145, 1219, 1314, 1340, 1363, 1445, 1588, 2192 (C=C)
ATTO725	728	978, 1102, 1165, 1224, 1289, 1341, 1365, 1399, 1456, 1506, 1596, 1738, 2228 (¹² C≡ ¹⁴ N)
BF4	735	1163, 1183, 1222, 1266, 1326, 1358, 1438, 1496, 1577, 2187 (C=C)
MARS2228 (BF1)	743	998, 1043, 1109, 1203, 1265, 1311, 1371, 1429, 1487, 1508, 1598, 1737, 2145 (¹³ C≡ ¹⁵ N), 2170 (¹³ C≡ ¹⁴ N), 2195 (¹² C≡ ¹⁴ N), 2220 (¹² C≡ ¹⁴ N)
Alexa 750	749	998, 1100, 1206, 1368, 1516
Cy7	750	1096, 1145, 1217, 1280, 1309, 1401, 1449, 1578
Alexa 790	782	1102, 1121, 1209, 1370, 1522
Cy7.5	788	1106, 1156, 1206, 1242, 1281, 1362, 1400, 1472, 1572

Note: Vibrational peaks were extracted from well-resolved absorption peaks from FTIR spectra of bulk samples or 10 mM solutions in DMSO. Vibrational peaks labelled in red have been

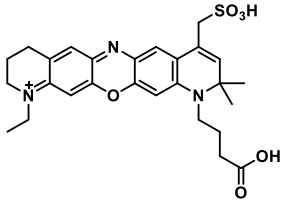
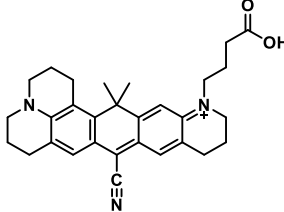
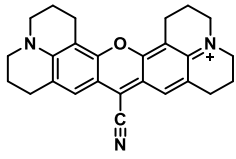
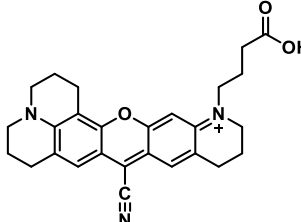
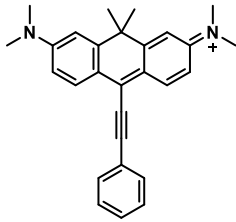
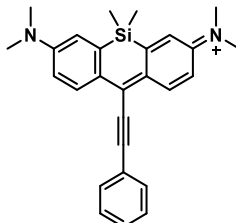
experimentally reproduced in BonFIRE spectroscopy, respectively. Except for ATTO680 (data in **Fig. 2f**), Rh800 (data in **Extended Data Fig. 9**), and BF2 (with a structure similar to Rh800, see **Table S3**), FTIR and available BonFIRE spectra data can be found in **Extended Data Fig. 3**.

Table S2. BonFIRE signal comparison of dyes with C=C modes.

Dye	Absorption peak (nm)	IR frequency (cm ⁻¹)	Probe wavelength (nm)	Measured BonFIRE strength
Nile Blue A	635	1580	705	0.02
ATTO647N	650	1598	720	0.29
ATTO665	673	1598	740	0.10
ATTO680	685	1598	765	1.00
BF2	688	1598	760	0.71
Rh800	696	1598	775	0.50
ATTO725	742	1598	825	0.28
BF1	758	1598	840	0.26

Note: For Nile Blue A, ATTO647N, and ATTO665, the dichroic/filter set of FF700-Di01/ FF01-650/60 (Semrock) was used; For ATTO680, BF2, and Rh800, the dichroic/filter set of FF738-FDi01/FF01-665/150 was used; For ATTO725 and BF1, the dichroic/filter set of FF801-Di01/FF01-709/167 was used. Absorption peaks were verified with UV-vis and FTIR measurements in DMSO solutions. Probe wavelengths were optimized so that the sum energy of IR + probe matches the absorption peak (The 705 nm for Nile Blue A was not optimized due to the limitation of the used dichroic mirror). BonFIRE experimental data were taken from 1 μ M solutions in DMSO.

Table S3. Molecular structures of dyes used in BonFIRE.

Name in the main text	Commercial name	Name in reference	Structure
ATTO680	ATTO680	-	
BF1	-	MARS2228 ⁶	
Rh800	Rh800	-	
BF2	-	MARS2238 ⁶	
BF3	-	Compound 1a ⁷	
BF4	-	Compound 1b ⁷	

Note: We renamed the dyes to BonFIRE (BF) series, focusing on their IR properties rather than the Raman counterparts. ATTO dyes were purchased from ATTO-Tec, GmbH. Rh800 was purchased from Sigma Aldrich. Cyanine dyes were purchased from Lumiprobe. Alexa dyes were

purchased from Thermo Fisher. BF dyes were synthesized according to the literature cited in the third column. Isotopologues of BF1 and BF2 were synthesized according to ref. ⁶. Available structures of other commercially available dyes (ATTO series, Alexa series, Cyanine series, etc.) used in BonFIRE could be found on the corresponding vendor's websites.

Table S4. BonFIRE signal comparison of dyes with C≡C and C≡N modes conjugated to the dye systems.

Dye	Absorption peak (nm)	Absorption coefficient (M ⁻¹ cm ⁻¹)	IR frequency (cm ⁻¹)	IR absorption coefficient (M ⁻¹ cm ⁻¹)	Calculated Franck-Condon factor	Quantum yield	Calculated BonFIRE strength relative to BF1	Measured BonFIRE strength
BF2	678	56078	2224 (C≡N)	28	0.08	0.16	0.41	0.59
BF3	680	39811	2194 (C≡C)	307	0.06	0.017	0.25	0.27
Rh800	687	66833	2224 (C≡N)	28	0.078	0.16	0.47	0.63
BF4	712	56234	2188 (C≡C)	351	0.043	0.004	0.07	0.83
ATTO725	728	123423	2224 (C≡N)	63	0.059	0.1	0.93	0.80
BF1	743	120000	2224 (C≡N)	70	0.059	0.1	1.00	1.00
BF1	743	120000	1598 (C=C)	3852	0.036	0.1	34	83

Note: For BF2, BF3, Rh800, and BF4, the dichroic/filter set of FF801-Di01/FF01-709/167 (Semrock) was used; For ATTO725 and BF1, the dichroic/filter set of Di02-R830/FF01-775/140 (Semrock) was used; Absorption peaks and cross sections were verified with UV-vis measurements on dye solutions in PBS. BonFIRE data were obtained from 1 μM PBS solution of each dye. Absorption peaks, coefficients, and quantum yields of BF3 and BF4 were obtained from ref. ⁷. ORCA and custom scripts were used to estimate Franck-Condon factors according to ref. ⁸. The last row (grey-shaded) of BF1 C=C was added for comparison.

Table S5. Comparisons of key parameters of bioimaging between BonFIRE, SREF, and FEIR

Parameter	BonFIRE	FEIR	SREF
Working conditions	$\omega_{\text{vib}} + \omega_{\text{probe}} \approx \omega_{\text{abs}}$	$\omega_{\text{vib}} + \omega_{\text{probe}} \approx \omega_{\text{abs}}$	$\omega_{\text{pump}} - \omega_{\text{Stokes}} = \omega_{\text{vib}};$ $2\omega_{\text{pump}} - \omega_{\text{Stokes}} \approx \omega_{\text{abs}};$ $1400 \text{ cm}^{-1} < \omega_{\text{abs}} - \omega_{\text{pump}} < 4200 \text{ cm}^{-1}$
Laser system	Two OPOs and one DFG	One OPA	One OPO
Repetition rate	80 MHz	1 MHz	80 MHz
Pulse width	2 ps	200~300 fs	~ 2 ps
Laser bandwidth	8 cm^{-1}	120 cm^{-1}	~ 10 cm^{-1}
Spectral measurement	Laser tuning, bond-selective	Interferometric, broadband	Laser tuning, bond-selective
Laser tunability for optimal Spectral coverage	$\omega_{\text{vib}}: 800 - 4200 \text{ cm}^{-1}$ $\omega_{\text{probe}}: 690 - 980 \text{ nm}$	$\omega_{\text{vib}}: \text{demonstrated around } 1600 \text{ cm}^{-1}$ $\omega_{\text{probe}}: 517 \text{ nm, fixed}$	$\omega_{\text{vib}}: \sim 1600 \text{ cm}^{-1};$ $\sim 2200 \text{ cm}^{-1}$ $\omega_{\text{probe}}: 700 - 750 \text{ nm};$ 788-834 nm with frequency-doubled idler beam
Objective	25X, NA 1.05	63X, NA 0.8	60X, NA 1.2
Resolution	600 nm	Not available	400 nm
Bioimaging compatibility	Yes	Challenging due to sample damage from high peak powers	Yes
Sensitivity	Single-molecule imaging with bio-compatibility	Single-molecule in acetonitrile- d_3 solution	Single-molecule imaging with bio-compatibility
Widefield compatibility	Yes	N/A	Point-scanning
Lifetime for sensing	Yes, bond-selective	Not demonstrated	Not available
Background source	Anti-Stokes (constant for a fixed ω_{probe}); Photothermal (removable with temporal subtraction)	Anti-Stokes (constant for a fixed ω_{probe}); Photothermal (removable with temporal subtraction)	Anti-Stokes (from both ω_{pump} and ω_{Stokes} , varying for different ω_{vib}); two-photon pump/Stokes combined excitation;
Background-free bioimaging	Demonstrated with fast AC modulation	N/A	Possible with a complex frequency modulation scheme

* We note that the previous vibrational super-multiplexing techniques (e.g., epr-SRS or Carbow) are limited to sensitivities of 250-500 nM, without single-molecule sensitivity for accessing low-abundance biomolecules.

References

- 1 Whaley-Mayda, L., Guha, A., Penwell, S. B. & Tokmakoff, A. Fluorescence-Encoded Infrared Vibrational Spectroscopy with Single-Molecule Sensitivity. *Journal of the American Chemical Society* **143**, 3060-3064 (2021). <https://doi.org:10.1021/jacs.1c00542>
- 2 Xiong, H. *et al.* Stimulated Raman excited fluorescence spectroscopy and imaging. *Nature Photonics* **13**, 412-417 (2019). <https://doi.org:10.1038/s41566-019-0396-4>
- 3 Shi, L., Hu, F. & Min, W. Optical mapping of biological water in single live cells by stimulated Raman excited fluorescence microscopy. *Nature Communications* **10**, 4764 (2019). <https://doi.org:10.1038/s41467-019-12708-2>
- 4 Deb, P. *et al.* Correlating Nitrile IR Frequencies to Local Electrostatics Quantifies Noncovalent Interactions of Peptides and Proteins. *The Journal of Physical Chemistry B* **120**, 4034-4046 (2016). <https://doi.org:10.1021/acs.jpcc.6b02732>
- 5 Bagchi, S., Fried, S. D. & Boxer, S. G. A Solvatochromic Model Calibrates Nitriles' Vibrational Frequencies to Electrostatic Fields. *Journal of the American Chemical Society* **134**, 10373-10376 (2012). <https://doi.org:10.1021/ja303895k>
- 6 Wei, L. *et al.* Super-multiplex vibrational imaging. *Nature* **544**, 465-470 (2017). <https://doi.org:10.1038/nature22051>
- 7 Pastierik, T., Šebej, P., Medalová, J., Štacko, P. & Klán, P. Near-Infrared Fluorescent 9-Phenylethynylpyronin Analogues for Bioimaging. *The Journal of Organic Chemistry* **79**, 3374-3382 (2014). <https://doi.org:10.1021/jo500140y>
- 8 Lee, S.-Y. & Heller, E. J. Time-dependent theory of Raman scattering. *The Journal of Chemical Physics* **71**, 4777-4788 (1979). <https://doi.org:10.1063/1.438316>